

25 *inclusion of illite and quartz did not have a significant influence on the form of the*
26 *relationship between stress and flow, i.e. both described by a power-law.*

27 **Keywords**

28 *Fracture flow; hydraulic flow; kaolinite; Ball Clay; shear testing; stress history; carbon*
29 *capture and storage.*

30

31 **1.0 Introduction**

32 Discontinuities (fracture, faults, joints, interfaces, etc.) play a pivotal role in controlling the
33 movement of water and gas in many geological settings. Depending on their orientation,
34 displacement, mineral composition and stress regime discontinuities can be the controlling
35 structural feature retarding the flow of hydrocarbons in conventional environments,
36 containing super-critical CO₂ in sequestration projects, and movement of gas and/or water in
37 radioactive waste disposal. Discontinuities can vary significantly in age. Normal faults acting
38 as hydrocarbon traps may have formed millions of years ago, whereas subsidence induced
39 faulting/fracturing in the same basin will have formed during the depletion of the reservoir.
40 Therefore in many geological settings both natural and induced discontinuities will have
41 formed.

42 Fluid flow in argillaceous materials, whether through the bulk rock or along discontinuities,
43 is closely related to the mechanical state of the caprock. In particular, the role of faults and
44 fractures as potential conduits or barriers to fluid flow is likely to be of critical importance to
45 seal integrity in Carbon Capture and Storage (CCS) sites. In addition, recent studies [Zoback
46 & Gorelick, 2012] and on-going developments relating to induced seismicity [Green, *et al.*
47 2011] in other industries have also highlighted the importance of a thorough understanding of
48 the potential for, and controls on, fault reactivation behavior.

49 In particular, fault-sealing of caprocks is likely to be heavily influenced by the presence of
50 clays along the slip surface. The sealing properties of inactive faults are well known in the
51 hydrocarbons industry and may arise through the presence of clay-rich gouge or through
52 hydrothermal cementation. For fault-valve behavior to take place, a fault must cut across a
53 vertical fluid pressure gradient which exceeds the hydrostatic gradient. The fault becomes
54 conductive when shear stress and/or pore pressure is sufficient. The consequent upward
55 discharge of fluids along the fault from the overpressured zone continues until the entire
56 hydraulic gradient reverts to hydrostatic conditions, or until the fault reseals. This also alters
57 the frictional shear resistance across the impermeable barrier.

58 Faulted geological settings are complex systems that are borne out of multiple episodes of
59 deformation, in the form of faulting, subsidence and exhumation, and altered stress regimes.
60 This means that faults cannot be viewed as static features over geological time. Nor can they
61 be considered static on CO₂ injection time scales, as complex pore-pressure histories and
62 chemical alteration-driven deformation may also have an impact on caprock systems. As
63 such, time is a significant factor in fault sealing.

64 On the long time-scales of interest in CCS, cross-reservoir fluid migration may lead to
65 changes in stress-state long after injection ceases. The response of new or previously-sealed
66 discontinuities exposed to these dynamic conditions, may be significant. Noy *et al.* [2012]
67 demonstrated that pore-pressure perturbations, resulting from the injection of CO₂, may
68 persist for significant periods (~300 years) after the injection phase. These perturbations are
69 likely to be particularly large in magnitude within the immediate vicinity of injection, but are
70 also demonstrably of concern ‘a considerable distance outside the CO₂ footprint at the end of
71 the injection period’. This raises a number of uncertainties in relation to the interaction of
72 fluids with caprock faulting, including the role of: (i) pre-existing discontinuities in the
73 caprock (either natural or reservoir-depletion-induced) with the potential to transmit fluids

74 under an elevated pore-pressure condition, (ii) critically oriented faults with the potential for
75 reactivation (as compared to those far from critically stressed), or faulting with the potential
76 for infrequent but significant seismicity.

77 Additionally, both near- and far-field discontinuities may be exposed to a range of changing
78 fluid chemistries during the evolution of a storage site, from CO₂-rich fluids to the migration
79 of brines at the periphery of the pressure pulse. In contrast to reservoir rocks, the
80 phenomenon of clay swelling is of major importance to the sealing behavior of argillaceous
81 cap-rocks [Horseman *et al.*, 2005; Tsang *et al.*, 2005], with the potential to notably affect
82 transmissivity of discontinuities. CO₂ has been shown to markedly impact on the swelling
83 properties of clays [Espinoza & Santamaria, 2012], but there is a paucity of data relating to
84 the impact on shale swelling properties and, in particular, the potential effects for fault
85 sealing behavior.

86 The permeability of rocks has been widely reported under hydrostatic stress conditions [e.g.
87 Zoback and Byerlee 1975; Walsh and Brace 1984; Morrow *et al.*, 1984; David *et al.*, 1994;
88 Dewhurst *et al.*, 1999^{a,b}; Katsube, 2000; Katsube *et al.*, 1996^{a,b}; Kwon *et al.*, 2001; Neuzil *et al.*
89 *et al.*, 1984 etc] in order to establish the relationship between effective stress and permeability
90 for different rock types. However, in the field, rocks are normally subjected to an anisotropic
91 stress-field, where the vertical stress (determined by the weight of the overburden) exceeds
92 the two horizontal stresses [Holt, 1990]. This has led to investigations of the sensitivity of
93 matrix permeability to non-hydrostatic stress conditions, especially in sandstones [e.g.
94 Keaney *et al.*, 1998; Zhu and Wong, 1994; Zhu and Wong, 1997]. The reported permeability
95 for intact shale, mudstones, and clay aggregates subjected to hydrostatic pressures varies
96 from 10⁻¹⁶ m² to 10⁻²³ m² [Kwon *et al.*, 2001]. Many researchers have shown that the
97 permeability of shale decreases with externally applied stress [Dewhurst *et al.*, 1999^{a,b};
98 Katsube, 2000; Katsube *et al.*, 1996^{a,b}; Kwon *et al.*, 2001; Neuzil *et al.*, 1984] and decreased

99 porosity [Dewhurst *et al.*, 1998; Schloemer and Kloss, 1997]. A number of non-linear
100 relationships have been proposed between permeability, porosity, and pressure in shale and
101 mudstones, including exponential and power laws between permeability and pressure
102 [Dewhurst *et al.*, 1999a; Katsube *et al.*, 1991].

103 Gutierrez *et al.* [2000] investigated experimentally the hydromechanical behavior of an
104 extensional fracture in Kimmeridge Shale under normal and shear loading. It was shown that,
105 at the time it was created, the fracture probably had about nine orders of magnitude higher
106 permeability than the permeability of the intact shale. Increasing the normal stress across the
107 fracture reduced the fracture permeability following an empirical exponential law. However,
108 loading the sample to an effective normal stress twice as much as the intact rock unconfined
109 compressive strength did not completely close the fracture, although it did reduce the
110 permeability by an order of magnitude. Cuss *et al.* [2011] showed that fracture transmissivity
111 in Opalinus Clay (OPA) decreased linearly with an increase in normal load over a limited
112 stress range. This study also showed that shearing was an effective self-sealing mechanism in
113 OPA and reduced hydraulic fracture transmissivity to similar levels to that of the intact
114 material. Cuss *et al.* [2014^{a,b}] reported a one order of magnitude reduction in fracture
115 transmissivity of OPA just in response to re-hydration of the fracture. A further order of
116 magnitude reduction was observed in response to shearing along the fracture.

117 The current study represents the first stage of a three-part investigation of the potential for
118 fault reactivation during the sequestration of carbon dioxide. The three parts of the study
119 were; 1) the role of stress history on fault flow properties; 2) quantification of fault
120 reactivation potential as a result of elevated pore pressure; and 3) the role of stress history on
121 fault reactivation. As a consequence of part (2) of the experimental program, the current
122 reported study investigated the hydraulic flow properties of a clay-filled discontinuity at 30°
123 to horizontal to cyclic changes in vertical load. Two clay gouges were selected so as to

124 investigate any potential changes in fault reactivation potential in part (2) of the study. The
125 objectives of the current study were:

- 126 • Investigate the relationship between stress and fault transmissivity;
- 127 • Investigate the role of stress history on fault transmissivity;
- 128 • Compare results from two clay gouges (kaolinite and Ball Clay).

129 This would simulate effective stress changes, such as pore-pressure variations on faults
130 during CO₂ sequestration or stress relaxation through exhumation. Previous experimental
131 work at the British Geological Survey (BGS) on fracture transmissivity in Opalinus clay
132 [Cuss *et al.*, 2009; 2011; 2014^{a,b}] and kaolinite gouge [Sathar *et al.*, 2012] showed that
133 hydraulic flow is a complex, focused, transient property that is dependent upon normal stress,
134 shear displacement, fracture topology, fluid composition, and clay swelling characteristics.
135 The current experimental program aimed to extend this knowledge by investigating the
136 influence of vertical stress cycling on hydraulic flow through gouge filled discontinuities.

137 Perturbations of the stress field are likely in many geological scenarios and the influence this
138 has on the flow properties of faults is important in determining the hydrogeological response
139 of the subsurface. This study was aimed to answer the question of whether stress history is of
140 importance in fault flow and whether the current stress state will dictate the flow properties of
141 faults. The study also aimed to answer whether variations in pore pressure as a result of CO₂
142 sequestration would alter the transport properties of existing faults within reservoirs. Should
143 stress history be observed, the flow properties of the faults would be dictated by the stress
144 state at which they were formed, not necessarily the current stress state and this adds
145 confidence that pore pressure variations during sequestration would not result in leakage.

146 **2.0 Experimental setup**

147 All experiments were performed using the bespoke Angled Shear Rig (ASR, Figure 1)
148 designed and built at the BGS. Previous experiments conducted on Opalinus Clay [Cuss *et*
149 *al.*, 2009; 2011; 2014] showed that fracture topology is a key parameter in controlling fluid
150 flow along fractures. In order to reduce the number of variables required to fully understand
151 flow, a “generic” discontinuity with smooth fracture surfaces was investigated.

152 The ASR (Figure 1) comprised of 5 key components:

- 153 1. Rigid body that had been designed to deform as little as possible during the experiment;
- 154 2. Vertical load system comprising an Enerpac hydraulic ram that was controlled using a
155 Teledyne/ISCO 260D syringe pump, a rigid loading frame and an upper thrust block
156 (with capacity of up to 20 MPa vertical stress, 72 kN force). The Enerpac ram had a
157 stroke of 105 mm, which meant that it could easily accommodate the vertical
158 displacement of the top block as it rode up the fault surface at constant vertical load.
159 Note: The vertical stress created by the ram is not equal to the normal stress perpendicular
160 to the fault plane and represents the maximum principal stress within the reservoir;
- 161 3. Shear force actuator comprised of a modified and horizontally mounted Teledyne/ISCO
162 500D syringe pump designed to drive shear as slow as 14 microns a day at a constant rate
163 (equivalent to 1 mm in 69 days) along a low friction bearing. Note that no shearing was
164 conducted in the current study;
- 165 4. Pore pressure system comprising a Teledyne/ISCO 500D syringe pump that could deliver
166 either water up to a pressure of 25.8 MPa. The syringe pump delivered water through the
167 center of the top block directly to the fault surface.
- 168 5. A state-of-the-art custom designed data acquisition system using National Instruments
169 LabVIEW™ software facilitating the remote monitoring and control of all experimental
170 parameters.

171 The experimental fault assembly consisted of precision machined 316 stainless steel top and
172 bottom blocks (thrust blocks) with a dip of 30 degrees with respect to horizontal. The thrust
173 blocks were polished so as not to introduce preferential pathways for flow. The top block was
174 connected to the vertical loading arrangement by means of a swivel mechanism which was
175 engaged to the shoulders on either side of the top block. Care was taken in the design of the
176 swivel mechanism so as to negate rotation and tilting of the top blocks and shear mechanism.
177 Two pore pressure transducers, attached to ports which were positioned orthogonally to each
178 other at 15 mm from the central pore fluid inlet, allowed measurement of pore pressures
179 within the fault gouge (see Figure 1). The thrust blocks of the apparatus were made with a
180 contact area of 60 mm × 60 mm. The lower thrust block was longer than the top one so that
181 the contact area of the experimental discontinuity could be maintained constant during a
182 shear test.

183 Vertical movement of the upper thrust block was measured by a high precision non-contact
184 capacitance displacement transducer, which had a full range of ± 0.5 mm and an accuracy of
185 $0.06 \mu\text{m}$. Horizontal load was measured using a load cell fitted laterally to the top-block. This
186 measured the force resultant from lateral movement of the bottom block transmitted through
187 the clay gouge.

188 Gouge material for the experiments was prepared from either powdered kaolinite or Ball Clay
189 (as described in Table 1); 16 ± 0.1 g of de-ionized water was added to 20 ± 0.1 g of oven
190 dried clay powder. The water and clay were then stirred for five minutes giving a fully
191 saturated paste. The mixed paste was smeared uniformly onto the surface of the top block,
192 which was then carefully lowered onto the bottom block thus forming a paste gouge. The
193 initial thickness of the gouge is usually of the order of 1 mm. However, as no lateral
194 confinement was made of the clay gouge, thickness decreased to approximately $70 \pm 10 \mu\text{m}$
195 with loading up to 10 MPa and clay was squeezed from between the thrust blocks; this excess

196 material stopped water from the shear bath entering the fault gouge or causing. The apparatus
197 was designed without lateral gouge confinement as this would require sealing elements that
198 would have a high frictional component along the fault surface compared with the low
199 frictional properties of the clay.

200 Two experiments are described in this paper (Table 2). Both were conducted from a low
201 vertical stress of approximately 0.4 MPa up to a maximum of 10 MPa. Each step was
202 approximately 1 day in length, with vertical stress increased instantaneously. Steady-state
203 flow had been achieved during this time, as seen by a constant transmissivity. Experience
204 from previous studies [Sathar *et al.*, 2012] showed that this length was sufficient and is an
205 appropriate compromise between overall test duration and attainment of steady-state flow.
206 Throughout the experiment deionized water was injected at a pore pressure of 1 MPa by
207 means of an ISCO/Teledyne syringe pump. The volume of the pump was monitored, giving
208 information on the flow rate of the injection system. Flow rate could then be converted to
209 transmissivity for the clay gouge. Fracture transmissivity is calculated assuming radial flow
210 from the injection hole given the steady state fluid flow rate Q and the pressure head H at the
211 injection point. Steady flow in a cylindrical geometry is given by:

$$212 \quad Q = \frac{2\pi T(h_i - h_o)}{\ln(r_o) - \ln(r_i)} \quad \text{Equation 1}$$

213 where T is the transmissivity, h_i is the head on the inner surface with radius r_i , and h_o is the
214 head on the outer surface at radius r_o (Gutierrez *et al.*, 2000). For the current experimental
215 setup $r_o = 30$ mm, $r_i = 1.96$ mm, $h_o = 0.05$ m (5 cm depth of water in the ASR bath) and $h_i \sim$
216 100 m (1 MPa injection pore pressure). Substituting these values into equation 1 and
217 rearranging allows transmissivity ($\text{m}^2 \text{s}^{-1}$) to be simply calculated from:

218
$$T = 1.183 \times 10^{-12} \frac{Q}{P_p}$$
 Equation 2

219 if the fluid flux (Q in $\mu\text{l h}^{-1}$) and pore pressure (P_p in kPa) are known. This relationship was
220 used to calculate the transmissivity of the fracture throughout the experiment. Average
221 flowrate and standard deviation for each step was calculated from six hours of flow data prior
222 to the final hour of each step.

223 3.0 Experimental results

224 Two tests with a test history of load-unload-reload-unload (LURU) are reported here, both
225 conducted on a 30° slip-plane (Table 2).

226 Figure 2 shows the data recorded during the LURU experiment for test ASR_BigCCS_01
227 conducted on kaolinite clay gouge. The test consisted of 44 stages. Vertical stress was
228 sequentially increased in stages of approximately 0.4 or 0.8 MPa per day to a maximum
229 vertical stress of 6.5 MPa (Figure 2a). During the unloading stage the vertical stress was
230 reduced in 0.2, 0.4 or 0.8 MPa steps per day to 0.1 MPa. This was followed by reloading in
231 0.4, 0.8 or 2 MPa steps to a vertical stress of 10 MPa, followed by unloading in 0.1, 0.4, 0.8
232 or 1.3 MPa steps to 0.1 MPa. The pore fluid injection pressure was maintained at a constant
233 value of 1 MPa. Temperature varied between at 20.4 and 21.1 $^\circ\text{C}$ throughout the duration of
234 the experiment, although this did not affect the experimental results (Figure 2b). The flow
235 rate decreased by a factor of 6 from $87 \mu\text{l h}^{-1}$ to $15 \mu\text{l h}^{-1}$ during loading from 0 to 6.5 MPa
236 (Figure 2c,d). Each test stage was approximately 1 day in duration. Previous studies [e.g.
237 Sathar *et al.*, 2012] had shown that this was sufficient to achieve steady-state conditions.
238 Ideally test stages should have been longer given the sensitivity of the Teledyne/ISCO pumps
239 to resolve such low flows. However, a compromise had to be taken to obtain data within a
240 realistic timeframe. During unloading from 6.5 to 0.1 MPa, flow rate remained essentially

241 unchanged at $14.8 \mu\text{l h}^{-1}$. During the first stage of reloading from 0.1 to 2 MPa, flow reduced
242 from $14.8 \mu\text{l h}^{-1}$ to $9.4 \mu\text{l h}^{-1}$, however, during reloading to the previous maximum stress of
243 6.4 MPa flow only marginally reduced from $9.4 \mu\text{l h}^{-1}$ to $9 \mu\text{l h}^{-1}$. Continued loading
244 following attainment of a stress condition greater than previously experienced resulted in
245 flow reducing to approximately $6.5 \mu\text{l h}^{-1}$. During the second unloading cycle to 0.1 MPa
246 flow did not recover until vertical stress was lower than 0.4 MPa, with flow increasing to
247 only $8.7 \mu\text{l h}^{-1}$ at a low vertical stress of 0.1 MPa. Pore pressure within the slip plane recorded
248 much lower pressures (6 – 26 kPa and 0 – 8 kPa) than the injection pressure (1 MPa) (Figure
249 2e), with P_1 initially decreasing during the first ten days of the experiment. Fracture width
250 reduced from an initial $160 \mu\text{m}$ to approximately $80 \mu\text{m}$ during the initial loading history
251 (Figure 2f). As seen, this reduction in fracture thickness is fully recovered during unloading.
252 The second loading stage reduced the fracture thickness to $60 \mu\text{m}$, with full recovery
253 observed again. This suggests that no loss of gouge occurred following the initial loading
254 step.

255 Figure 3 shows the data recorded during the LURU experiment for test ASR_BigCCS_02
256 conducted on Ball Clay gouge. The test consisted of 34 stages. Vertical stress was
257 sequentially increased in stages of approximately 0.4 or 0.8 MPa per day to a maximum
258 vertical stress of 6.4 MPa (Figure 3a). During the unloading stage the vertical stress was
259 reduced in 0.4 or 0.8 MPa steps per day to 0.4 MPa. This was followed by reloading in 0.4 or
260 0.8 MPa steps to a vertical stress of 8.5 MPa, followed by unloading in 1 or 2 MPa steps to
261 0.4 MPa. The pore fluid injection pressure was maintained at a constant value of 1 MPa.
262 Temperature remained relatively uniform at $19.5 \pm 0.1 \text{ }^\circ\text{C}$ throughout the duration of the
263 experiment, although a step in temperature was seen around Day 20 that did not affect the
264 experimental results (Figure 3b). The flow rate decreased by a factor of 4 from $40 \mu\text{l h}^{-1}$ to 9
265 $\mu\text{l h}^{-1}$ during loading from 0 to 6.5 MPa (Figure 3c,d). During unloading from 6.5 to 0.4 MPa,

266 flow rate remained essentially unchanged from $9 \mu\text{l h}^{-1}$ to $8.6 \mu\text{l h}^{-1}$. During reloading from
267 0.4 MPa to the previous maximum stress of 4.6 MPa, flow remained approximately constant,
268 until a stress condition greater than previously experienced, with flow decreasing to $6.7 \mu\text{l h}^{-1}$.
269 During the second unloading cycle to 0.4 MPa flow did not recover, even at low vertical
270 stresses. Pore pressure within the slip plane recorded much lower pressures (32 – 38 kPa)
271 than the injection pressure (1 MPa) and were generally stable throughout the experiment
272 (Figure 3e). Figure 3f shows that fracture thickness was initially 210 μm in thickness, with
273 initial loading reducing this to approximately 60 μm . Unloading of the fault only recovered
274 thickness to 75 μm . Reloading resulted in fracture thickness reducing to 35 μm , with a
275 recovery to 53 μm . Both unloading stages did not fully recover fracture thickness, suggesting
276 that gouge and/or water was expelled during the test history.

277 Figure 4 shows the results of flow achieved for two tests conducted injecting water into a 30°
278 discontinuity during initial loading and unloading stages. As can be seen, the reduction in
279 transmissivity (T) during increasing vertical stress (σ_v) can be described by the following
280 power-law relationships:

281 Kaolinite: $T = 3.809 \sigma_v^{-0.415} \quad R^2 = 0.979$

282 Ball Clay: $T = 2.659 \sigma_v^{-0.514} \quad R^2 = 0.985$

283 Table 3 shows R^2 values for the fit of data for both tests using cubic, exponential, linear,
284 logarithmic, and power-law relationships; all of which have previously been proposed to
285 describe the relationship between stress and fault transmissivity. The power-law gives the
286 best fit for three of the four conditions modelled, although exponential, logarithmic and cubic
287 laws also fit the data well. As the power-law gave the best fit for the current data, especially
288 in the early stages of loading, we propose this as a description of fault transmissivity with

289 stress. The colation of more datasets will give a better understanding of the relationship
290 between stress and fault flow.

291 Figure 4 shows the change in transmissivity with decreasing vertical stress during the first
292 unloading stage. As can be seen both kaolinite (Figure 4a) and Ball Clay (Figure 4c) show
293 similar behaviour with transmissivity essentially unchanged, even when vertical stress was
294 reduced to 0.07 MPa during test ASR_BigCCS_01. This demonstrates that the clay has
295 considerable hysteresis and “memory” of the maximum stress that was experienced. Figure
296 4c compares the results achieved for kaolinite and Ball Clay. Both clays give a good power-
297 law relationship with an exponent of -0.5, with variation in the base number; 4.44 and 2.59
298 for kaolinite and Ball Clay respectively. No significant variation in gouge thickness was
299 noted between the tests (see Figure 7c). Therefore the difference in the base number is related
300 to the difference in mineralogy between the two tests.

301 Figure 5 shows the complete data for test ASR_BigCCS_01 conducted on kaolinite gouge.
302 As can be seen, increasing vertical stress resulted in a reduction in flow. During reloading,
303 continued increases of vertical stress up to 6.45 MPa, the previous maximum vertical stress,
304 did not result in any further reduction in flow. As vertical stress increased to a new maximum
305 in the test history, transmissivity continued to decrease following a power-law relationship.
306 Vertical stress was increased to a maximum of 10 MPa, resulting in a transmissivity of $0.75 \times$
307 $10^{-14} \text{ m}^2 \text{ s}^{-1}$. As shown in Figure 4b, reloading of the fault does not result in any change in
308 transmissivity until a new maximum stress has been achieved. Close examination of all data
309 shows that the first stage of reloading, increasing vertical stress from 0.7 to 2 MPa resulted in
310 slip along the fault plane. This was detected as a slight change in shear stress and vertical
311 displacement. No other change in vertical stress resulted in a slip event. It is possible to
312 correct this influence, as shown by the black arrows in Figure 5b, with corrected reload data
313 shown by open diamond symbols. The resulting relationship is shown in Figure 5c, with a

314 power-law describing the reduction of flow properties during increasing vertical stress
315 conditions and a linear constant relationship describing the behaviour when vertical stress
316 was reduced.

317 Figure 6 shows the complete data for test ASR_BigCCS_02 conducted on Ball Clay gouge.
318 As seen in Figure 6a and in more detail in Figure 6b, reloading followed a path similar to that
319 seen during unloading. Transmivity data for unloading from 6.45 MPa to 0.42 MPa gives an
320 average of $0.93 \times 10^{-14} \text{ m}^2 \text{ s}^{-1}$ compared with an average of $0.91 \times 10^{-14} \text{ m}^2 \text{ s}^{-1}$ during
321 reloading from 0.42 MPa to 6.45 MPa. Therefore it can be concluded that flow is 'identical'
322 during unloading and reloading and no change, either increase or decrease occurs.
323 Throughout the unload-reload history the gouge has a memory of the maximum stress it has
324 experienced. Only one further step was conducted after the previous maximum 6.45 MPa,
325 therefore it cannot be determined if transmissivity continued to decrease as described by a
326 power-law. However, as seen in Figure 6, the loading stages of the experiment are well
327 described by a single power-law relationship. The second unload stage of the experiment
328 resulted in no change in transmissivity.

329 Figure 7 shows the results of flow achieved for the two tests conducted injecting water into a
330 30° discontinuity during load-unload-reload-unload stages. As can be seen, the reduction in
331 transmissivity (T) during increasing vertical stress (σ_v) can be described by power-law
332 relationships. In all four stages with decreasing vertical stress it was seen that transmissivity
333 remained constant and reloading resulted in no variation in flow unless slip or a new
334 maximum stress state was achieved. Figure 7c shows the results for fracture thickness during
335 the experiment. For kaolinite a general linear reduction in fracture width was seen, whereas in
336 Ball Clay a form similar to that seen in flow was observed. This suggests that a component of

337 flow is related to fracture thickness, with an additional component related to the compaction
338 behavior of the clay gouge.

339 **4.0 Discussion**

340 The sequestration of super-critical carbon dioxide will result in pore pressure perturbations of
341 the injected reservoir. This will result in elevated pore pressure at faults, reducing effective
342 stress, and may result in super-critical CO₂ coming into contact with existing faults. The
343 current study utilized water as the injection fluid, so as to directly simulate the pressure pulse
344 of the reservoir within the existing pore fluid. The configuration of the angled shear rig did
345 not allow super-critical CO₂ to be injected; the injection of super-critical CO₂ at vertical
346 stress up to 10 MPa at 20° C would result in the instantaneous conversion to a gaseous form,
347 which would not occur in reality. However, the fluid nature of super-critical CO₂ should
348 behave similarly to water, although it may have an increased influence on flow as it reacts
349 with the clay gouge.

350 The current experimental study utilized a kaolinite or Ball Clay gouge as an analogue for a
351 clay-filled fault. This was in order to reduce the number of variables in the experiments by
352 effectively eliminating fracture roughness and the presence of asperities. The selection of
353 kaolinite was guided by the low swelling capacity of the clay, facilitating quicker
354 experiments and the study of a greater number of features of fracture flow. Ball Clay was
355 selected as it has a kaolinite content of 37 %, along with 35 % illite and 26 % quartz. This
356 was deemed to be sufficiently different in terms of mineralogy than pure kaolinite to observe
357 whether mineralogy played a role on fracture flow properties and behavior. If such an
358 observation was made then further research would be needed to fully quantify the role of
359 mineralogy on fault flow behavior.

360 Comparisons can be seen between the current experiments and those conducted on fractures
361 in Opalinus Clay (OPA). Cuss *et al.* [2009; 2011] describe the variation of fracture flow
362 dependence on normal stress for an idealized planed fracture. A hydraulic transmissivity of
363 approximately $5 \times 10^{-14} \text{ m}^2 \cdot \text{s}^{-1}$ was observed in OPA, which is comparable with the $0.5 - 5 \times$
364 $10^{-14} \text{ m}^2 \cdot \text{s}^{-1}$ seen in the current study. Fracture transmissivity in a realistic fracture in OPA has
365 been shown to reduce in a similar form to the current study [Cuss *et al.*, 2012; 2014^{1,2}]. These
366 observations therefore show that the use of a kaolinite or Ball Clay gouge can be seen to have
367 been justified given the similarity seen in response.

368 It was seen in test ASR_BigCCS_01 that flow reduced during the first step of reloading,
369 possibly as a result of shear. Fracture transmissivity was seen to reduce in OPA as a result of
370 shear for a planed fracture [Cuss *et al.*, 2009; 2011] and for a realistic fracture [Cuss *et al.*,
371 2012; 2014^{1,2}]. Cuss *et al.* [2014¹; 2014²] showed that shear reduced fracture transmissivity
372 by approximately one order of magnitude. Cuss *et al.* (2013) also showed that shear was an
373 effective self-sealing mechanism in kaolinite paste with a 40 % reduction in flow seen as a
374 result of shear. This compares with the 60 % reduction in flow seen during test
375 ASR_BigCCS_01. The fracture width and vertical displacement data suggest that movement
376 did occur, although movement was of the order of 10's microns. Previous studies have shown
377 that active shearing is an effective self-sealing mechanism that occurs in naturally fractured
378 claystone, such as Opalinus Clay, and in clay gouge material, such as kaolinite. The current
379 data suggest that only small shear movements are sufficient to alter the flow properties of
380 clay-rich gouge. This is not too surprising given the nano- to micro-scale of clay minerals. As
381 no further movements along the fracture plane were observed, the correction of the
382 transmissivity data shown in Figure 5b was possible to remove the influence of shear.
383 Therefore it is suggested that a small slip event occurred as vertical stress was increased by 2
384 MPa, which resulted in a reduction of flow properties.

385 The current study has highlighted the significance of stress history. The behavior observed
386 during unloading was similar for both tests during all four unloading stages. Considerable
387 hysteresis was seen during the unloading cycles of the test history with transmissivity
388 remaining constant with a memory of the maximum load experienced. Similar hysteresis has
389 been noted in Opalinus Clay [Cuss *et al.* 2009; 2011]; whilst the data were not described in
390 terms of hysteresis, a reinterpretation of the data shows that hysteresis was indeed observed.
391 This illustrates the importance of stress history on predicting flow along discontinuities and
392 has been used to explain the non-applicability of the critical stress approach in its simple
393 form at the Sellafeld site in the UK [Sathar *et al.*, 2012]. Therefore stress history is an
394 important control on fracture flow and consideration only of the current stress state will lead
395 to inaccuracies of the flow of fractured rocks.

396 During unloading and reloading it can be argued that the amount of flow recovered is
397 effectively zero, even when vertical stress is reduced to very small magnitudes. During
398 unloading of a deformed sediment only the elastic deformation is recovered and the stress
399 path followed corresponds to the rebound-reconsolidation line (RRL) or the swelling-
400 recompression line (SRL) under drained conditions. The form of the flow seen during cyclic
401 loading suggests that the clay paste follows the normal consolidation line (NCL) during
402 loading, with considerable hysteresis seen as the clay follows the SRL during unloading and
403 reloading, until the NCL is once again reached, from where the plastic deformation occurs,
404 following the NCL. The NCL and RRL are usually defined in the effective stress versus void
405 ratio (e) space, therefore fracture transmissivity observed is related to the change in void ratio
406 as the gouge consolidates in response to the vertical stress. This consolidation takes the form
407 of a power-law relationship. However, as shown in Table 3, an exponential, cubic or
408 logarithmic fit can also achieve satisfactory fits to the data. The power-law relationship gives
409 the best fit to the data in the early stages of initial loading, as shown in Figure 8..

410 The load-unload-reload-unload experiments conducted on kaolinite and Ball Clay did not
411 significantly vary. The form of the transmissivity reduction with vertical stress was similar,
412 with differences noted in the fracture transmissivity seen at 6.5 MPa. This difference may
413 simply be related to differences in permeability of the two gouges and differences in gouge
414 thickness, although as shown in Figure 7c, the two tests achieved similar gouge thickness.
415 The illite content of Ball Clay is likely to have a lower permeability, as observed as a lower
416 fracture transmissivity. It should also be noted that the Ball Clay gouge resulted in a more
417 pronounced reduction in transmissivity with increased vertical stress; this will be related to
418 the differences in grain dimension, swelling potential, and permeability of the two gouge
419 materials. The minimum transmissivity seen after both clay gouges had been loaded to 10
420 MPa vertical stress was approximately 0.8 and $1.5 \times 10^{-14} \text{ m}^2 \text{ s}^{-1}$ for Ball Clay and kaolinite
421 respectively. Therefore the variation in mineralogy had resulted in variations in the power-
422 law reduction in flow and transmissivity at increased vertical stress, but did not alter the
423 unloading behaviour.

424 Faults within clay-rich caprock seals are likely to be of low permeability and this will affect
425 the drainage of the gouge during loading and unloading cycles. The current experiments were
426 all conducted as drained experiments, with a central 1 MPa pore pressure reducing to
427 atmospheric pressure at the outside of the sample. If the gouge was behaving as undrained, it
428 would be expected to see pore pressure increases at P1 and P2 as vertical stress was
429 increased. Modelling of the radial pressure distribution expected from such a geometry
430 predicts that pore pressure should be 250 kPa at the observation pressure ports, as shown in
431 Figure 9. This is greatly in excess of the measured pore pressure, which had a maximum of
432 35 kPa. This either suggests that pore pressure was not simply radial flow, or that channelised
433 flow occurred. Cuss *et al.* (2011) used fluorene tagged water to show that fracture flow in
434 Opalinus Clay exploited less than 50 % of the total fracture surface. This test was conducted

435 under static boundary conditions for over 100 days and attained full steady-state conditions;
436 therefore the localisation of flow and low pore pressure within the gouge cannot be simply
437 due to non-steady state flow. It is therefore possible that hydraulic flow is simply not
438 intersecting the two pore pressure monitoring locations. The use of an inclined fault plane at
439 30° would likely result in preferential flow down-dip, however, the location of P2 suggests
440 that this is not the case. This suggests that the dip of the plane plays little role on the flow
441 direction of the injected fluid. Unfortunately it is not possible to retrieve the gouge at the end
442 of the experiment to determine where fluid flow has been active. In nature the conditions are
443 likely to be drained, but if the stress change is rapid compared with the drainage rate, the
444 response may be akin to undrained testing. The observations seen of hysteresis during
445 unloading and the description of the stress path followed as an RRL response is likely to
446 occur under undrained conditions. However, increases in vertical stress are likely to create
447 elevated pore pressures, which results in a more complex permeability response with changes
448 in vertical stress.

449 **5.0 Conclusions**

450 This paper describes an experimental study of 2 load-unload-reload experiments, both on a
451 30° slip-plane filled with kaolinite or Ball Clay gouge. The main conclusions of the study
452 were;

- 453 a. The transmissivity of the Ball Clay and kaolinite gouge showed a power-law relationship
454 with stress between 0 and 10 MPa vertical stress.
- 455 b. During a loading (vertical stress) and unloading cycle considerable hysteresis in flow was
456 observed signifying the importance of stress history on fracture flow. Consideration of
457 just the current stress acting upon a fracture may result in inaccuracies of predicted water
458 flow;

- 459 c. During reloading a permeability response akin to the rebound-reconsolidation line was
460 observed until a stress state equivalent to the maximum stress experienced previously,
461 from where flow continued to reduce as the response now followed the normal
462 consolidation line.
- 463 d. Shear movement is an effective self-sealing mechanism that can reduce the transmissivity
464 of fractures with only small movements of the order of 10's microns needed to reduce
465 transmissivity.
- 466 e. No significant variation was seen in the relationship between stress and flow between
467 kaolinite and Ball Clay, with both well described by a power-law. This suggests the
468 inclusion of illite and quartz did not have a significant alteration to the relationship
469 between stress and flow. Ball Clay is likely to have a lower permeability than pure
470 kaolinite and this was observed as a lower fracture transmissivity, as seen by the power-
471 law coefficients.
- 472 f. Observations of flow within a clay-filled gouge were consistent with experiments
473 conducted on Opalinus Clay, showing that the simplified experimental geometry
474 effectively replicated the flow observed in real fractures.

475 **Acknowledgements**

476 The study was undertaken by staff of the Minerals and Waste Program of the BGS using the
477 experimental facilities of the Transport Properties Research Laboratory (TPRL). The authors
478 would like to thank the skilled staff of the Research & Development Workshops at the BGS,
479 in particular Humphrey Wallis, for their design and construction of the experimental
480 apparatus. This publication has been produced with support from the BIGCCS Centre. The
481 BIGCCS Centre is part of the Norwegian research programme Centres for Environment-
482 friendly Energy Research (FME) and is funded by the following partners: Aker Solutions,
483 ConocoPhillips, Det Norske Veritas, Gassco, Hydro, Shell, Statoil, TOTAL, GDF SUEZ and

484 the Research Council of Norway (193816/S60). The BGS authors publish with the
485 permission of the Executive Director, British Geological Survey (NERC).

486 **References**

487 Cuss, R.J., Sathar, S., and Harrington, J.F. (2013) Final Report of FORGE WP4.1.2:
488 Validation of critical stress theory applied to repository concepts. *British Geological Survey*
489 *Commissioned Report, CR/13/001*. 96pp.

490 Cuss, R.J., Milodowski, A.E., Harrington, J.F. and Noy, D.J. (2009) Fracture transmissivity
491 test of an idealised fracture in Opalinus Clay. British Geological Survey Commissioned
492 Report, CR/09/163. 74pp.

493 Cuss, R.J., Milodowski, A., and Harrington, J.F. (2011) Fracture transmissivity as a function
494 of normal and shear stress: first results in Opalinus clay. *Physics and Chemistry of the*
495 *Earth*. 36, pp. 1960-1971.

496 Cuss, R.J., Harrington, J.F., Milodowski, A.E., and Wiseall, A.C. (2014^a). Experimental
497 study of gas flow along an induced fracture in Opalinus Clay. British Geological Survey
498 Commissioned Report, CR/14/051. 79pp.

499 Cuss, R.J. and Harrington, J.F. (2014^b) Experimental observations of the flow of water and
500 gas along fractures in Opalinus Clay. Extended abstract We07. Fourth EAGE Shale
501 Workshop, 6-9 April 2014, Porto, Portugal.

502 Cuss, R.J., Harrington, J.F., Sathar, S., and Norris, S. (2015) An experimental study of the
503 flow of gas along faults of varying orientation to the stress-field; Implications for
504 performance assessment of radioactive waste disposal. *Journal of Geophysical Research –*
505 *Solid Earth*. 120, pp.3932-3945, doi:10.1002/2014JB011333

506 David, C., Wong, T.F., Zhu, W., and Zhang, J. (1994) Laboratory measurement of
507 compaction-induced permeability change in porous rocks; implications for the generation

508 and maintenance of pore pressure excess in the crust. *Pure and Applied Geophysics*, 143,
509 pp. 425-456.

510 Dewhurst, D.N., Aplin, A.C., and Sarda, J.-P. (1999) Influence of clay fraction on pore-scale
511 properties and hydraulic conductivity of experimentally compacted mudstones. *Journal of*
512 *Geophysical Research*, 104, pp. 29,261-29,274.

513 Dewhurst, D.N., Aplin, A.C., Sarda, J.-P., and Yang, Y. (1998) Compaction-driven evolution
514 of porosity and permeability in natural mudstones: An experimental study. *Journal of*
515 *Geophysical Research*, 103, pp. 651-661.

516 Dewhurst, D.N., Yang, Y., and Aplin, A.C. (1999) Permeability and fluid flow in natural
517 mudstones. In: Aplin, A.C., Fleet, A.J., and Macquaker, J.H.S., eds., *Mud and Mudstones:*
518 *Physical and Fluid Flow Properties*, Geological Society of London, Special Publications,
519 158, pp. 23-43.

520 Donohew, A.T., Horseman, S.T., and Harrington, J.F. (2000) Gas entry into unconfined clay
521 pastes at water contents between the liquid and plastic limits. in: *Environmental*
522 *Mineralogy: Microbial Interactions, Anthropogenic Influences, Contaminated Land and*
523 *Waste Management*; Cotter-Howells, J.D., Campbell, L.S., Valsami-Jones, E., and
524 Batchelder, M. (eds). *Mineralogical Society Series*, 9. Mineralogical Society, London. Pp.
525 369-394 ISBN 0 903056 20 8.

526 Espinoza, D. Nicolas, and J. Carlos Santamarina. (2012). Clay interaction with liquid and
527 supercritical CO₂: The relevance of electrical and capillary forces." *International Journal of*
528 *Greenhouse Gas Control*, 1, 351-362.

529 Green, C., Styles, P. and Baptie, B. (2011). Preese Hall Shale gas fracturing review and
530 recommendations for induced seismic mitigation, Independent Review, Pub. Department of
531 Energy and Climate Change, UK.

532 Gutierrez, M., Øino, L.E. and Nygard, R. (2000) Stress-dependent permeability of a de-
533 mineralised fracture in shale. *Marine and Petroleum Geology*, 17, pp.895–907.

534 Highley, D.E. (1984) *China Clay*. Mineral Dossier No. 26. Mineral Resources Consultative
535 Committee, HMSO, London.

536 Holt RM (1990) Permeability reduction induced by a non-hydrostatic stress field. *SPE*
537 *Formation Evaluation*, Dec 1990, pp. 444–448

538 Horseman, S. T., R. J. Cuss, and H. J. Reeves. (2005). Clay Club initiative: Self-healing of
539 fractures in clay-rich host rocks. In ‘Stability and Buffering Capacity of the Geosphere for
540 Long-term Isolation of Radioactive Waste’, Nuclear Energy Agency 117.

541 Katsube, T.J., Issler, D.R., and Coyner, K. (1996) Petrophysical characteristics of shale from
542 the Beaufort-Mackenzie Basin, northern Canada; permeability, formation factor, and
543 porosity versus pressure, Interior plains and Arctic Canada. *Current Research - Geological*
544 *Survey of Canada*. pp. 45-50.

545 Katsube, T.J., Boitnott, G.N., Lindsay, P.J., and Williamson, M. (1996) Pore structure
546 evolution of compacting muds from the seafloor, offshore Nova Scotia. In: Anonymous,
547 ed., *Eastern Canada and national and general programs*. *Current Research - Geological*
548 *Survey of Canada*, pp. 17-26.

549 Katsube, T.J. (2000) Shale permeability and pore-structure evolution characteristics.
550 *Geological Survey of Canada*. Ottawa, ON, Canada. Pages: 9.

551 Keaney, G.M.J., Meredith, P.G., and Murrell, S.A.F. (1998) Laboratory study of permeability
552 evolution in a 'tight' sandstone under non-hydrostatic stress conditions. *Rock Mechanics in*
553 *Petroleum Engineering*, 1 8-10 July 1998, Trondheim, Norway, Society of Petroleum
554 Engineers, SPE/ISRM 47265, pp. 329-335.

555 Kwon, O., Kronenberg, A.K., Gangi, A.F., and Johnson, B. (2001) Permeability of Wilcox
556 Shale and its effective pressure law. *Journal of Geophysical Research, B, Solid Earth and*
557 *Planets*, 106, pp. 19,339-19,353.

558 Morrow, C., Shi, L.Q., and Byerlee, J.D. (1984) Permeability of fault gouge under confining
559 pressure and shear stress. *Journal of Geophysics Research*, 89, pp. 3193-3200.

560 Neuzil, C.E., Bredehoeft, J.D. and Wolff, R.G. (1984) Leakage and fracture permeability in
561 the Cretaceous shales confining the Dakota aquifer in South Dakota. In: *Proceedings of*
562 *First C.V. Theis Conference on Geohydrology in Dublin, Ohio*. Jorgensen, D.G. and Signor,
563 D.C. (eds.). National Water Well Association. pp.113-120.

564 Noy, D.J.,Holloway, S., Chadwick, R.A., Williams, J.D.O., Hannis, S.A. and Lahann, R.W.
565 (2012). Modelling large-scale carbon dioxide injection into the Bunter Sandstone in the UK
566 Southern North Sea. *International Journal of Greenhouse Gas Control*, 9, 220–233.

567 Sathar, S., Reeves, H.J., Cuss, R.J., and Harrington, H.J. (2012) Critical stress theory applied
568 to repository concepts; the importance of stress tensor and stress history in fracture flow.
569 *Mineralogical Magazine*. December 2012, 76 (8), pp. 3165-3177.

570 Schloemer, S., and Krooss, B.M. (1997) Experimental characterisation of the hydrocarbon
571 sealing efficiency of cap rocks. *Marine and Petroleum Geology*, 14, pp. 565-580.

572 Tsang, C.-F., Bernier, F. and Davies, C. (2005). Geohydronechanical processes in the
573 Excavation Damaged Zone in crystalline rock, rock salt, and indurated and plastic clays—in
574 the context of radioactive waste disposal, *International Journal of Rock Mechanics &*
575 *Mining Sciences* 42, 109–12.

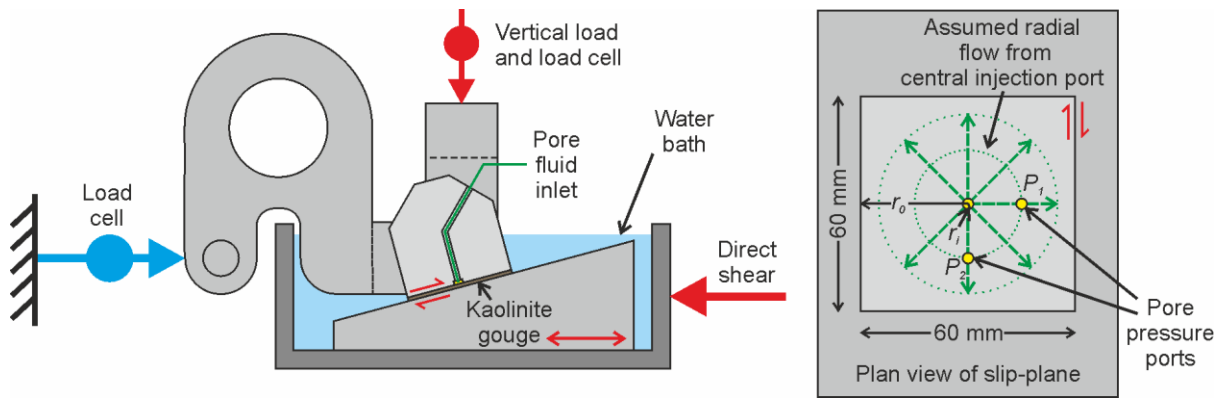
576 Walsh, J.B., and Brace, W.F. (1984) The effect of pressure on porosity and the transport
577 properties of rock. *Journal of Geophysical Research. B*, 89, pp. 9425-9431.

578 Zhu, W., and Wong, T.f. (1994) Permeability evolution related to the brittle-ductile transition
579 in Berea Sandstone. In: Anonymous, ed., AGU 1994 fall meeting., 75; 44 Suppl.: Eos,
580 Transactions, American Geophysical Union. pp. 638.

581 Zhu, W., and Wong, T.-f. (1997) The transition from brittle faulting to cataclastic flow;
582 permeability evolution. *Journal of Geophysical Research, B, Solid Earth and Planets*, 102,
583 pp. 3027-3041.

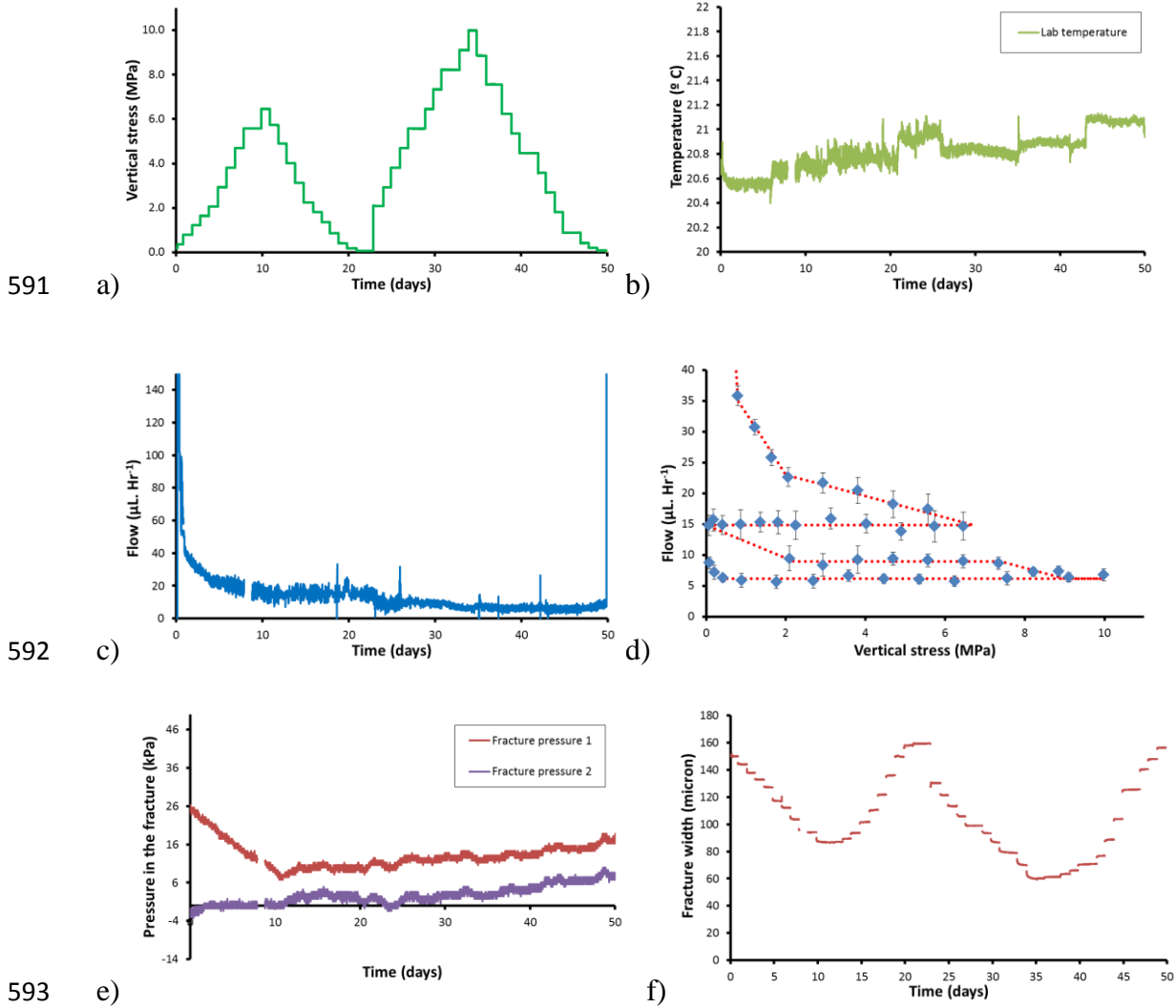
584 Zoback, M.D., and Byerlee, J.D. (1975) The effect of microcrack dilatancy on the
585 permeability of Westerly Granite. *Journal of Geophysics Research*, 80, pp. 752-755.

586 Zoback, D. and Gorelick, S. (2012). Earthquake triggering and large-scale geologic storage
587 of carbon dioxide. *Proceedings of the National Academy of Sciences* 109.26 (2012): 10164-
588 10168.

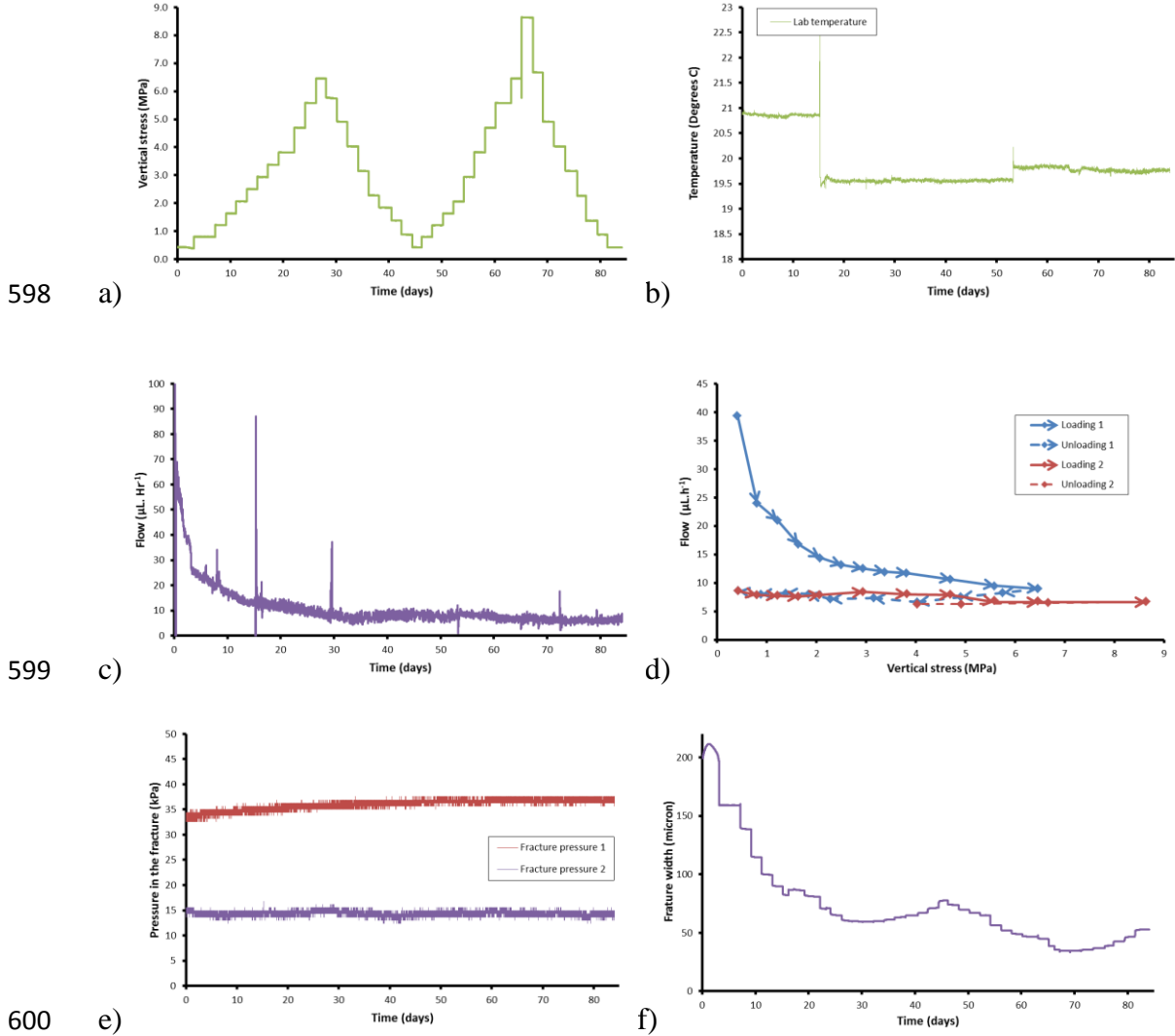


589

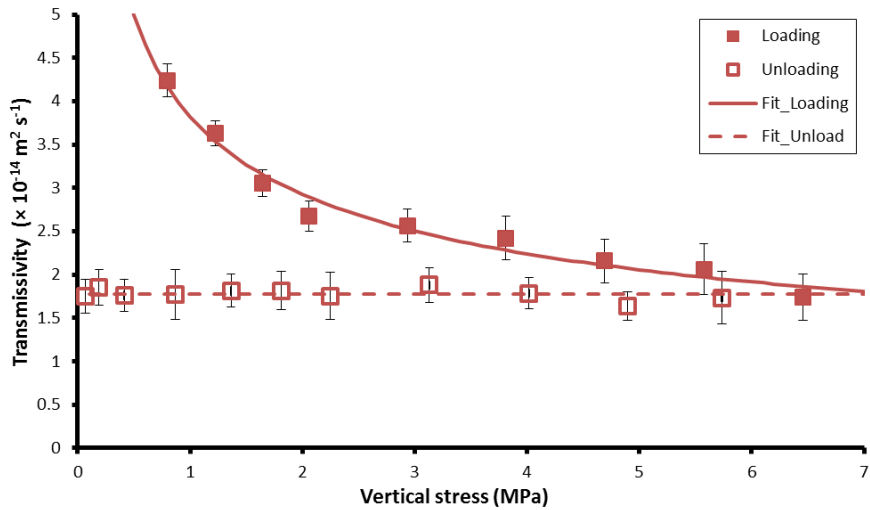
590 **Figure 1** Schematic of the Angled Shear Rig (ASR).



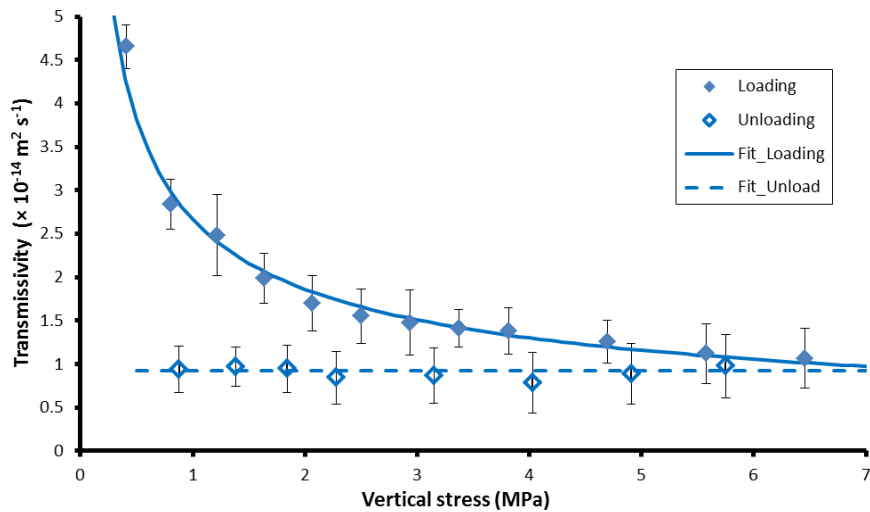
594 **Figure 2** Results from load-unload-reload-unload (LURU) test conducted on kaolinite
 595 (ASR_BigCCS_01): a) vertical stress; b) temperature; c) hydraulic flow with time; d)
 596 hydraulic flow variation with vertical stress; e) pore pressures within the slip plane at pore
 597 pressure ports P_1 and P_2 ; f) Fracture width.



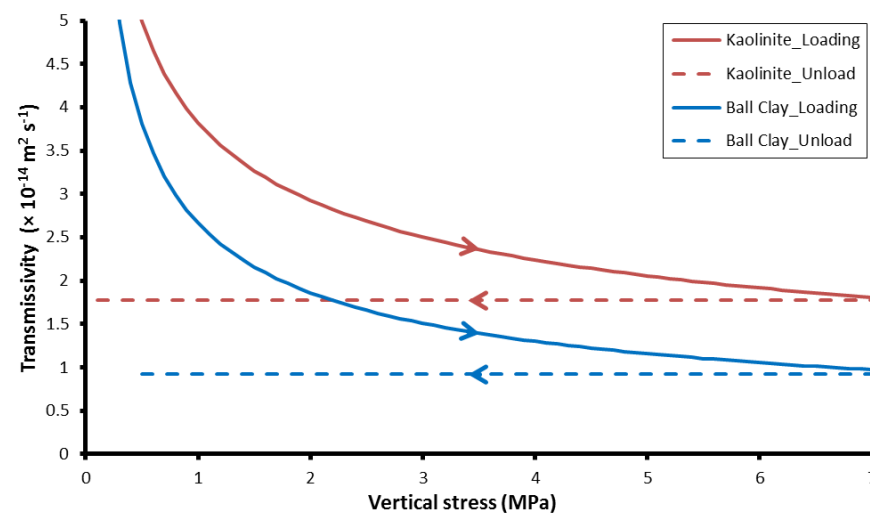
601 **Figure 3** Results from load-unload-reload-unload (LURU) test conducted on Ball Clay
 602 (ASR_BigCCS_02): a) vertical stress; b) temperature; c) hydraulic flow with time; d)
 603 hydraulic flow variation with vertical stress; e) pore pressures within the slip plane at pore
 604 pressure ports P_1 and P_2 ; f) Fracture width.



605 a)



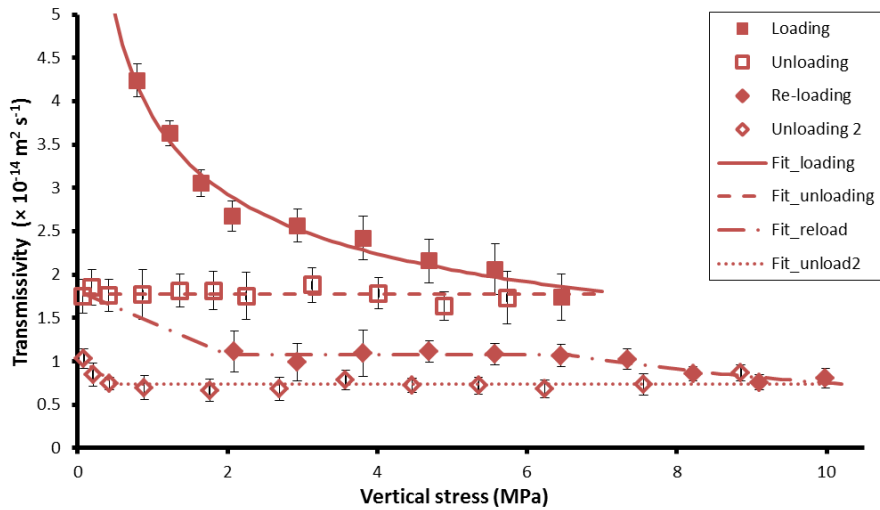
606 b)



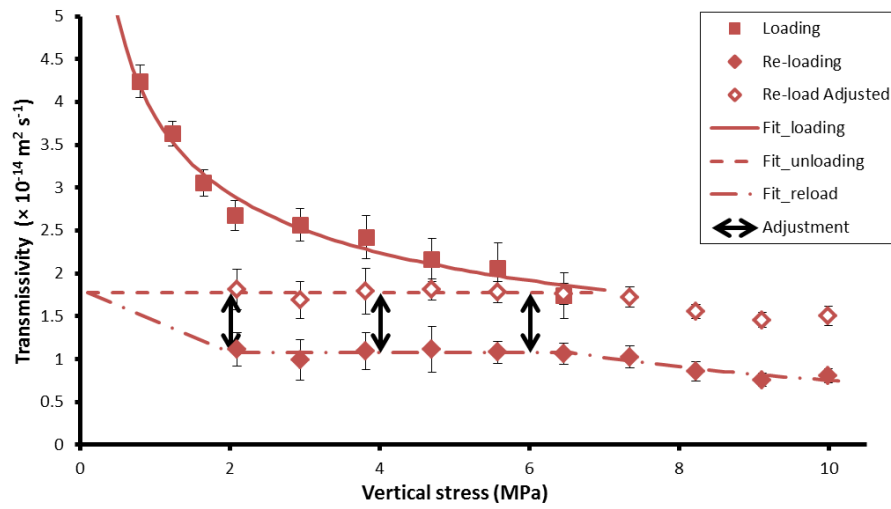
607 c)

608 **Figure 4** Example of hysteresis seen in flow during loading/unloading experiments on a
 609 30° slip-plane; a) kaolinite loading-unloading experiments; b) Ball Clay during loading-
 610 unloading-reloading experiments; c) comparison of kaolinite and Ball Clay during LU stages.

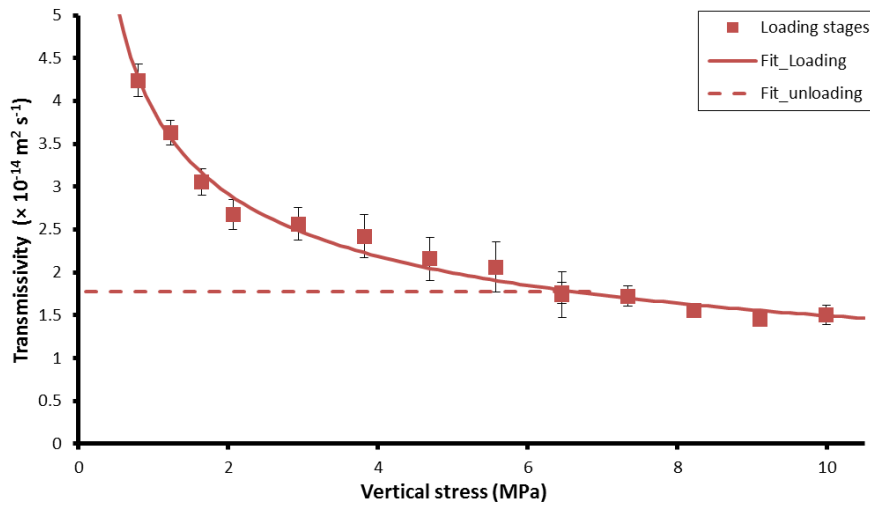
611 Note that error bars show the standard deviation observed in flow recorded over a 6 hour
612 period. This plot shows that flow reduces with increased load, but does not recover flow
613 during unloading.



614 a)



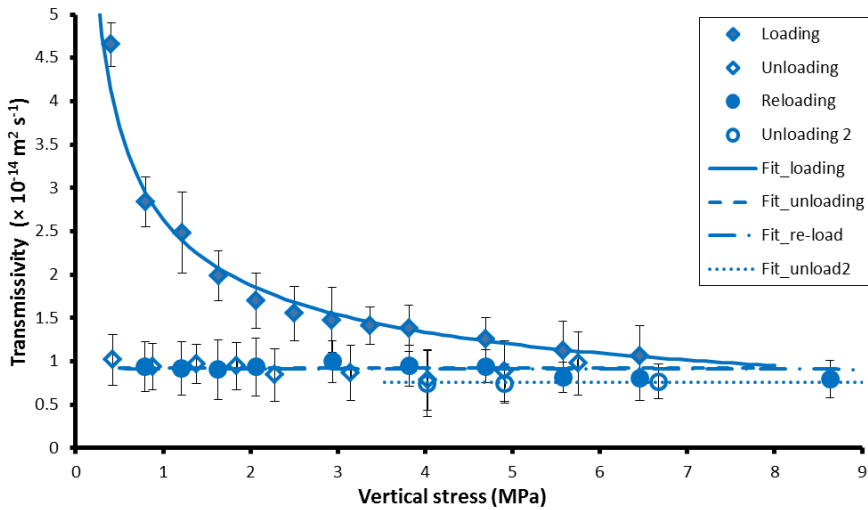
615 b)



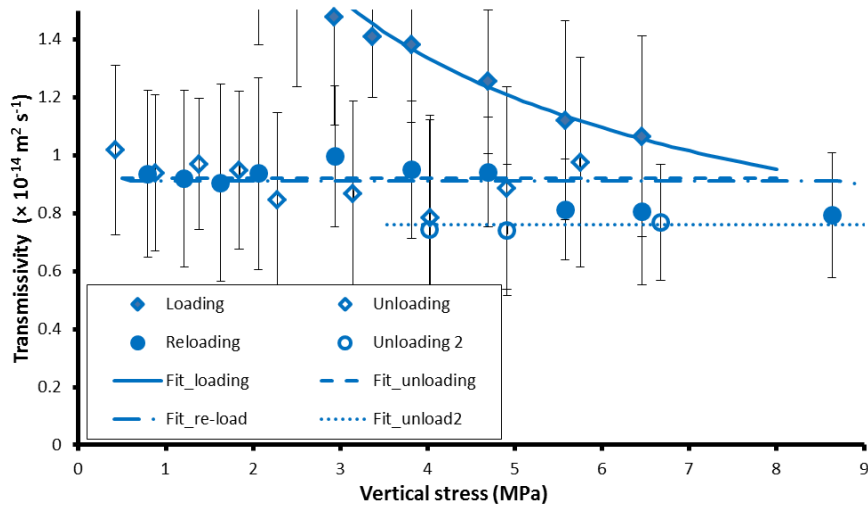
616 c)

617 **Figure 5** Results for reloading-unloading for test ASR_BigCCS_01 conducted on kaolinite
 618 gouge; a) complete transmissivity data; b) adjustment of reloading data (see text for
 619 explanation); c) adjusted results for complete LURU test. Note that error bars show the

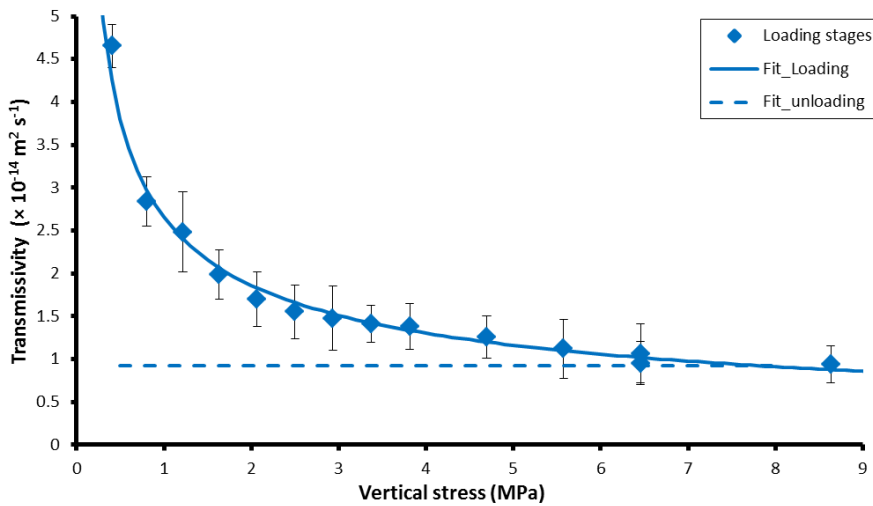
620 standard deviation observed in flow recorded over a 6 hour period. This plot shows no
621 increase in flow occurs during until a new maximum stress has been attained, demonstrating
622 that fault flow has a stress memory.



623 a)



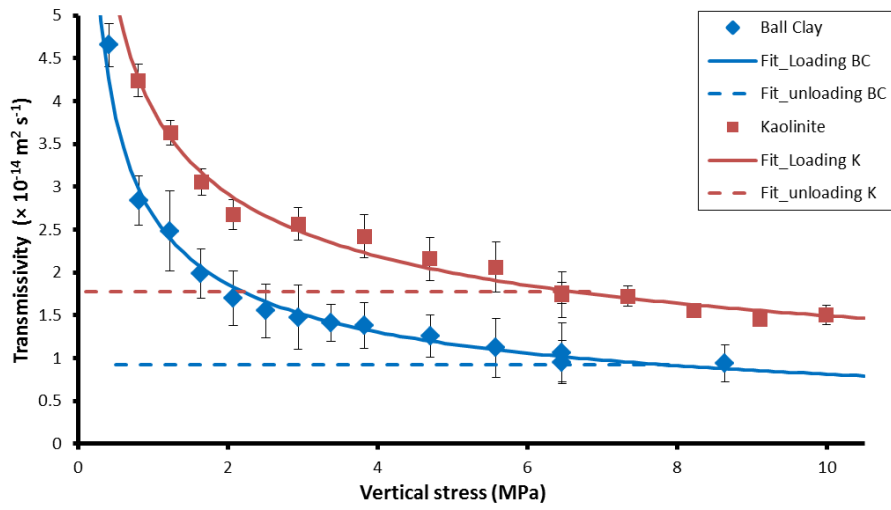
624 b)



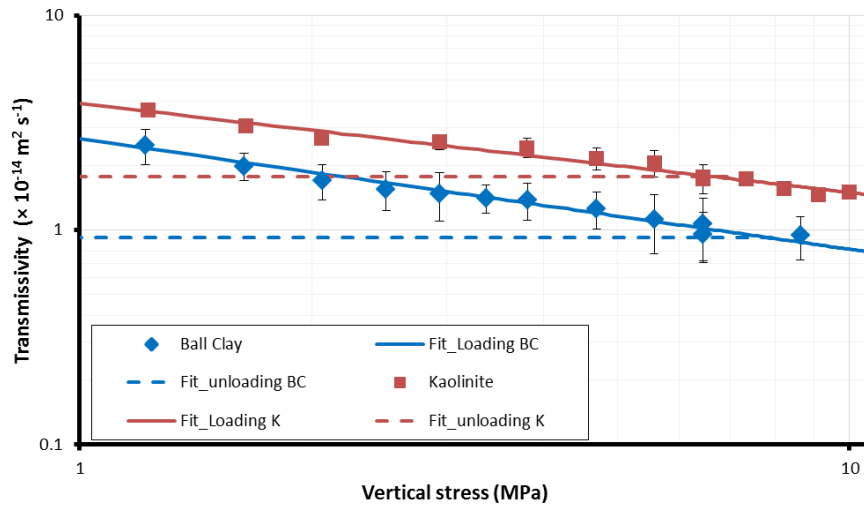
625 c)

626 **Figure 6** Results for reloading-unloading for test ASR_BigCCS_02 conducted on Ball
 627 Clay gouge; a) complete transmissivity data; b) detail of unloading and reloading stages; c)
 628 results for complete LURU test. Note that error bars show the standard deviation observed in

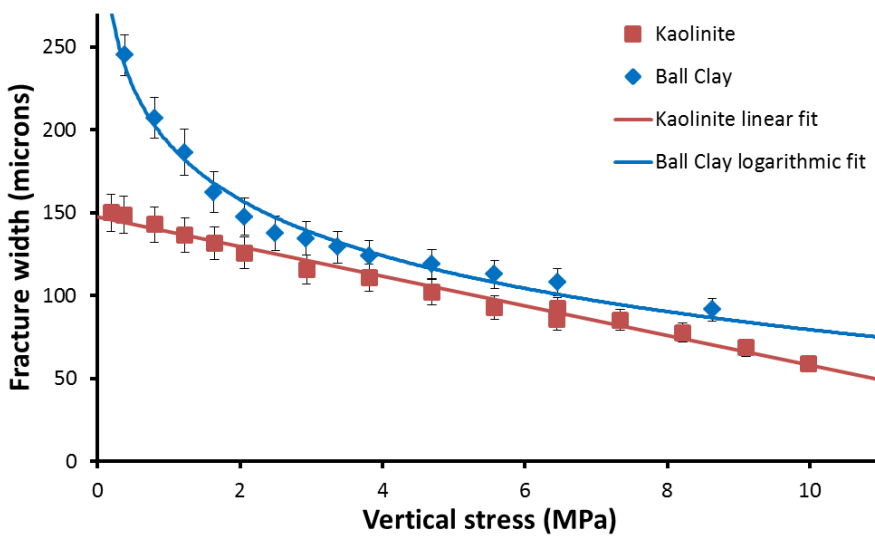
629 flow recorded over a 6 hour period. This plot shows no increase in flow occurs during until a
630 new maximum stress has been attained, demonstrating that fault flow has a stress memory.



631 a)

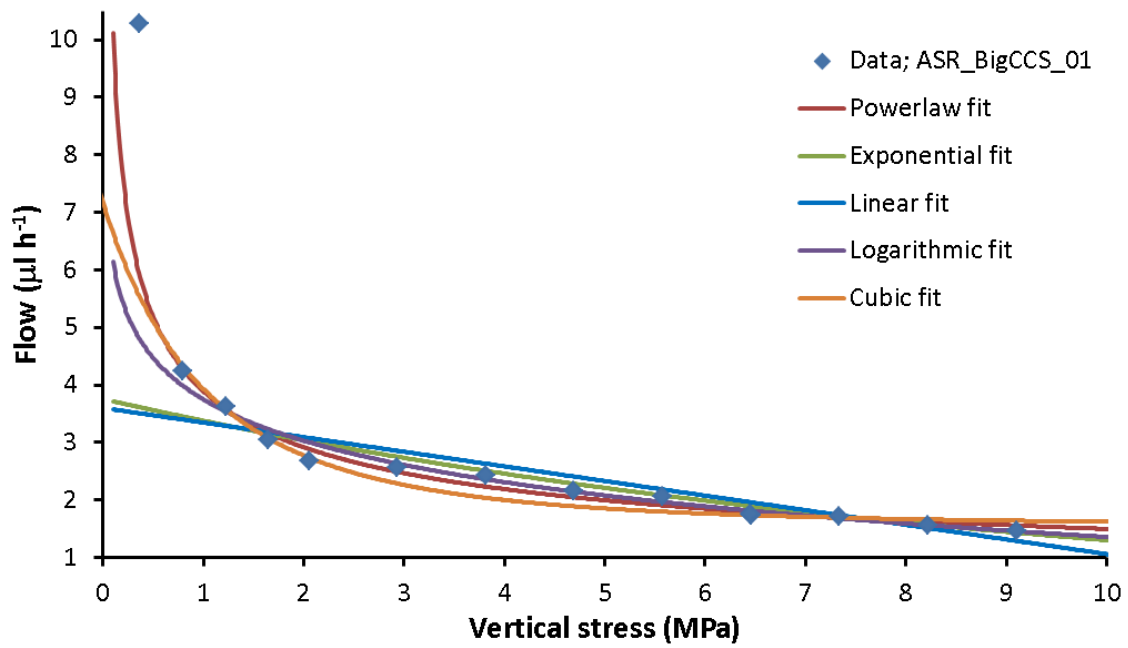


632 b)



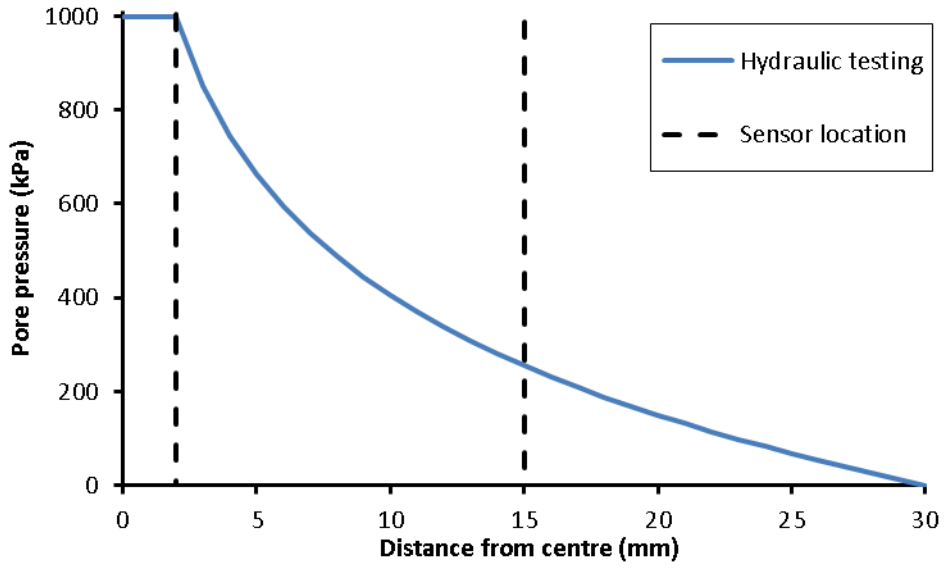
633 c)

634 **Figure 7** Comparing the loading-unloading-reloading response of kaolinite and Ball Clay
635 fault gouge material; a) power-law reduction in transmissivity seen during loading and stable
636 flow seen during unloading; b) data shown in the log-log space giving linear relationships of
637 transmissivity versus vertical stress; c) fracture width recorded during the experiment. Note
638 that error bars show the standard deviation observed in flow recorded over a 6 hour period.
639 This plot shows that loading can be represented by a power-law relationship, whilst
640 unloading shows no change in flow properties.



641

642 **Figure 8** Comparing five best-fit relationships to the experimental data of test
 643 ASR_BigCCS_01. The power-law fit is seen to best describe the data, especially at the initial
 644 loading stage at low vertical stress.



645

646 **Figure 9** Model of pore-pressure distribution in the clay gouge assuming radial flow.

Gouge	Supplier	Geological information	Location	Composition
Kaolinite	Imerys	well-ordered form, coarse hexagonal platelets ¹	St Austell, UK	100 % kaolinite
Ball Clay	Imerys	A1 seam; Tertiary, Poole Formation, Oakdale Clay Member)	Arne Clay Pit, Wareham, UK	37% kaolinite, 35% mica/illite and 26% quartz, together with some feldspar ²

647 **Table 1** Description of the clay gouge materials used during the current study. ¹ Highley,
648 (1984); ² Donohew et al. (2000).

	Experiment	Sample Material	Type of test	Slip-plane orientation
1	ASR_BigCCS_01	Kaolinite	LURU	30°
2	ASR_BigCCS_02	Ball Clay		

649 **Table 2** List of all experiments undertaken as part of the current study. ASR = Angled
650 Shear Rig; LURU = load-unload-reload-unload experiment.

Test	Material	Section	Cubic	Exp ¹	Linear	Log	Power
ASR_BigCCS_01	Kaolin	Load-reload	0.865	0.925	0.835	0.972	0.979
ASR_BigCCS_01	Kaolin	Unload	0.1	0.2	0.197	0.07	0.073
ASR_BigCCS_02	Ball Clay	Load-reload	0.973	0.783	0.573	0.888	0.985
ASR_BigCCS_02	Ball Clay	Unload	0.119	0.001	0.003	0.039	0.045

651 **Table 3.** Statistics for fit of data using different relationships. Values in bold represent the
652 best fit achieved.